2024 IEEE International Conference on Robotics and Automation (ICRA 2024)
May 13-17, 2024. Yokohama, Japan

Towards Visibility Estimation and Noise-Distribution-Based Defogging for LiDAR in Autonomous Driving

Jie Zhan[1], Yucong Duan[1], Junfeng Ding[1], Xuzhong Hu[1], Xiao Huang[2] and Jie Ma[1†]

***Abstract*— Point clouds play a crucial role in robots and intelligent vehicles. Noise caused by fog droplets seriously degrades the quality of point clouds. Previous researches have shown that the extent of degradation is correlated with visibility. The fog attenuation coefficient is associated with visibility. In light of this background, this paper proposes a noise-distribution-based defogging method for point clouds. Our approach hinges on the estimation of the fog attenuation coefficient, facilitated by road-based prior knowledge. Subsequently, our method integrates the fog-induced noise distribution inferred from the LiDAR imaging model with the spatially non-uniform distribution of point clouds caused by LiDAR structure. The fused results are input to a statistical filter based on the relative sparsity of noise to achieve defogging. This paper is one of the early works focusing on point cloud defogging. Its core insight lies in the estimation of the attenuation coefficient and the employment of fog-induced noise distribution for defogging. Experiments demonstrate that our method can accurately mitigate the impact of fog and meanwhile enhance the performance of 3D object detection network.**

I. INTRODUCTION

LiDAR is widely used in mobile robots and autonomous vehicles for perception. This is because LiDAR excels at measuring distance. In the future, Level 5 autonomous driving might rely on LiDAR point clouds for tasks like 3D object detection [1] [2], tracking [3] and Simultaneous Localization and Mapping (SLAM) [4]. The quality of point clouds greatly affects the stability of these algorithms.

Recently, experiments conducted in foggy weather [6] [8]–[10] [27] [28] have revealed that fog can lead to considerable distortion in point clouds. Typically, diameters of fog droplets are concentrated at the micrometer scale. This implies that when the laser beam of a Near-Infrared (NIR) wavelength LiDAR, commonly used in autonomous driving, illuminates the surfaces of these particles, Mie scattering takes place [5]. Fig. 1. shows the process of scattering. As shown in [8]–[10] [27] [30], the extent of fog distortion is related to visibility. Meanwhile, visibility is associated with the distribution of fog noise [12]. These correlations suggest that the estimation of visibility-related prior knowledge and noise distribution will be of great assistance in defogging.

Until now, researchers have proposed several methods to reduce the impact of fog in point clouds. Among these, [14] employs traditional filtering methods based on the sparsity of fog-induced noise. However, this approach does not take the non-uniform distribution of point clouds caused by LiDAR system into consideration. [13] attempts to extract characteristics from noise points. This method is deemed less appropriate for sparse point clouds collected outdoors. WeatherNet [15] demonstrates the ability to distinguish noise generated by rain and fog. Nevertheless, its stability relies on a large amount of point-wise labeled training data. Our goal is to identify defogging methods that provide interpretability. Snow removal techniques [19]–[22] based on relative sparsity of noise have attracted considerable attention. Their success indicates that this is a promising direction.

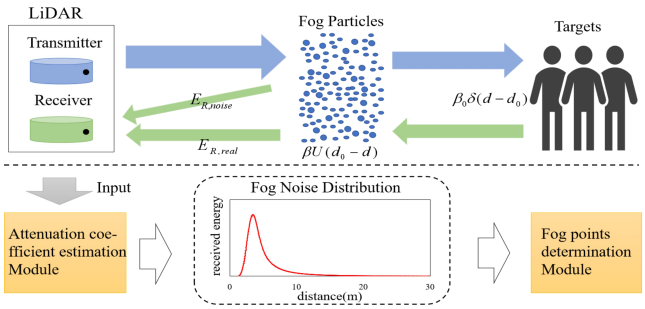

Fig. 1. Upper layer exhibits light propagation process of Mie scattering. Blue represents the forward channel while green represents the backward channel. The boldness of the arrows indicates the light energy. Low layer illustrates the workflow of our algorithm for processing foggy point clouds. The fog noise distribution curve is based on Eq. 12..

Developing a reasonable and effective algorithm for point cloud defogging is not a straightforward task. Firstly, the complexity of fog-induced noise poses a challenge. Solid defogging algorithms should consider physical models that encompass factors like light propagation and scattering process. Secondly, the sparsity and non-uniformity of LiDAR data may result in mistakenly filtering out real target points. Furthermore, in contrast to the wealth of prior knowledge available for image defogging, research on point cloud defogging is comparatively limited. This adds to the difficulty of the algorithmic design..

In this paper, we attempt to address the challenging defogging task by proposing a machine learning method. Initially, we propose an approach to estimate fog attenuation coefficient α using a single-frame point cloud. α reflects the density of fog and is vital for accurately representing fog-induced noise's distribution. By applying Koschmieder's law [31], one can straightforwardly calculate the well-known visibility from α. Taking cues from previous algorithms [14] [19] [20], our method integrate the acquired noise distribution with the non-uniform distribution of points caused by LiDAR structure. The combined result is then

† Corresponding author : majie@hust.edu.cn
[1]Authors are with School of Artificial Intelligence and Automation, Huazhong University of Science and Technology, Wuhan 430074, China. zhanjie@hust.edu.cn
[2]Author is with China Ship Development and Design Center, Wuhan 430064, China.

subjected to the Statistical Outlier Removal (SOR) [14] based on relative sparsity like [19]–[22]. This step is taken to fully exploit the sparsity and distribution characteristics of fog-induced noise. Consequently, our method eliminates points identified as noise, accurately reducing the adverse effects of fog.

Generally speaking, this paper's main contributions encompass three aspects:

- A framework for LiDAR point cloud defogging relies on visibility-related attenuation coefficient estimation and noise distribution in autonomous driving.
- A technique for estimating the fog attenuation coefficient in autonomous driving. This estimation roots in the combination of road prior knowledge and LiDAR imaging model for real targets.
- The first to propose an unsupervised machine learning defogging method based on the distribution of fog-induced points. We grasp the distribution of noise using LiDAR imaging model for fog particles. Then, the distribution information is implemented in a statistical filter .

II. RELATED WORK

Point cloud defogging is an emerging field with limited existing outcomes. In pursuit of comprehensiveness, our related work incorporates a segment of research focused on snow removal. These approaches not only contribute to our methodology but also serve as valuable references.

A. Effects of Fog on LiDAR

Researchers have investigated the impact of fog on point clouds from both physical model and real-world testing. Rasshofer *et al.* [5] established a fog-induced noise model for LiDAR. The authors analyze the influence of fog from a theoretical standpoint. The DENSE project [6] [8]–[10] [15] [28] has contributed a wealth of notable information to the study of LiDAR performance under foggy conditions. Researchers substantiate the degradation of point cloud through testing various LiDAR in foggy weather. [8]–[10] collected fog ruined data in a meticulously controlled adverse weather simulation environment in France. Their results powerfully indicate a correlation between noise distribution and visibility. Recently, researchers at Nagoya University, Japan, conducted field tests on the performance degradation of several commonly used LiDAR under foggy conditions, yielding similarly persuasive results [27].

B. Defogging Methods

Abu Ubaidah Shamsudin *et al.* [13] extract fog characteristics from point clouds and employ Support Vector Machines (SVM) for defogging. This approach was confined to indoor testing and lacked provision of training data. The derivation of fog characteristics requires a sufficiently dense set of points. This condition is challenging to meet for sparse point clouds in autonomous driving. The authors of [14] utilize traditional Statistical Outlier Removal (SOR) and Radius Outlier Removal (ROR) to filter noise based on the sparsity of fog-induced points. However, this method did not account for the non-uniform spatial distribution of the point cloud. WeatherNet [15] implements CNN to discriminate between fog and rain noise, with its robustness reliant on extensive and diverse training data. In contrast to deep learning approaches, we are inclined towards identifying methods with higher interpretability and universality for defogging. This will ensure the transferability across a range of scenarios.

C. Desnowing Methods

Compared to defogging, research on snow removal has garnered more attention. Snow noise is similarly sparse. Grounded in this characteristic, researchers have proposed the DROR [19] and DSOR [20]. These methods address the non-uniform spatial distribution of point clouds in comparison to the basic ROR and SOR [14]. Additionally, LIOR [22], DDIOR [21] and [24] are intensity-based snow removal techniques. Among these, [24] integrates effective information from a continuous sequence of frames. However, in dense fog scenarios, noise intensity can become comparable to that of real target points. This may result in grave errors when applying intensity-based denoising. Furthermore, deep learning-based approaches like LiSnowNet [23] and 4DenoiseNet [25] have achieved remarkable snow removal effects. LiSnowNet employs a more advanced noise representation model, while 4DenoiseNet constructs a deep learning network based on spatial and temporal information among multiple frames. More recently, SMEDNet [26] is considering multiple echoes as inputs. These snow removal methods provide valuable insights for our research.

III. METHODOLOGY

Fig. 2. illustrates our proposed framework for point cloud defogging. In this work, the estimation of fog attenuation coefficient α and fog-induced noise distribution occupies a core position. Section A introduces the LiDAR imaging background as the foundation for the estimation in Section B and C. Section D is the fog points determination module.

A. LiDAR Optical Model Background

Rasshofer *et al.* [5] pioneered the investigation of LiDAR imaging model in foggy weather for autonomous driving scenarios. They modeled the received signal E_R by using the temporal convolution between the transmitted signal E_T and the spatial transfer response function $H(d)$.

$$E_R(d) = C_A \int_0^{2d/c} E_T(t)\, H\left(d - \frac{ct}{2}\right) dt \tag{1}$$

In this equation, d is the distance of the response. C_A is the system constant related to the internal structure of LiDAR. In multi-beam LiDAR, the divergence of the beam and the asymmetry of electronic components lead to different system constants for each scanning layer [17]. E_T is typically defined in the following form:

$$E_T(t) = \begin{cases} E_0 \sin^2\left(\frac{\pi}{2\,\tau_H} t\right), & 0 \le t \le 2\,\tau_H \\ 0 \quad , & \text{otherwise.} \end{cases} \tag{2}$$

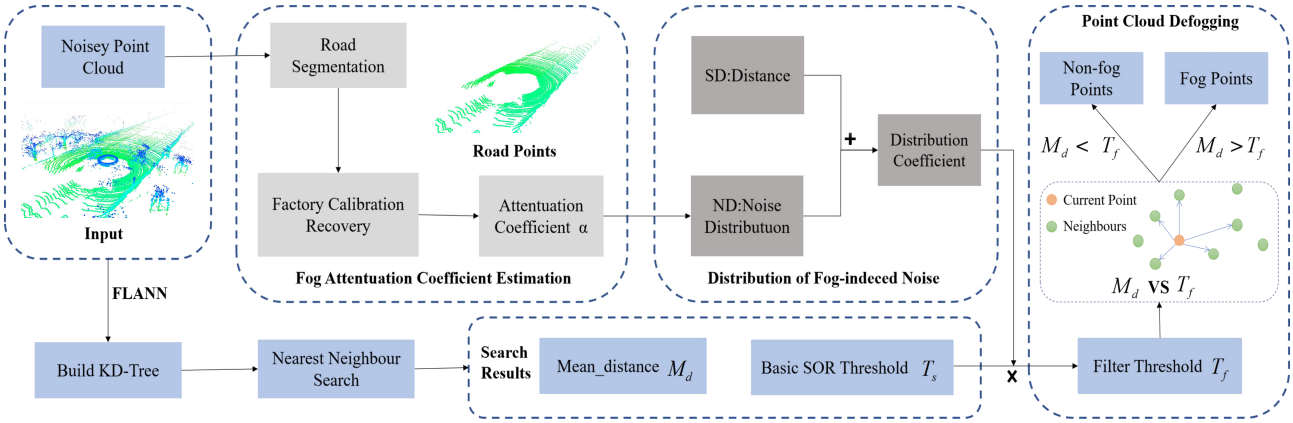

Fig. 2. Our framework includes the estimation step and noise removal step. The input noisy point cloud is initially processed by Section III.B to estimate attenuation coefficient α. It is then used to obtain the fog-induced Noise Distribution (ND). The fusion of ND with the Spatially non-uniform Distribution (SD) is utilized to determine the filtering threshold of the Statistical Outlier Removal (SOR). This filter employs K-Nearest Neighbor(KNN) search to calculate the mean distance of neighbors for each point and the global mean distance.

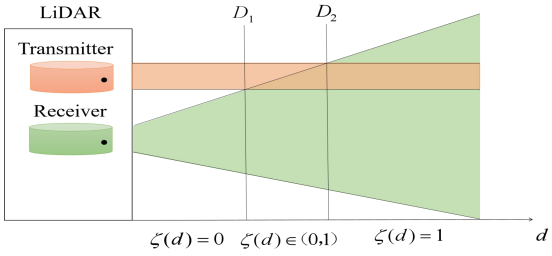

Fig. 3. The optical crossover function between transmitted and received laser. Figure adjusted from [5] and [16]

E_0 represents the peak value in transmitted signal pulse. τ_H stands for the half-wavelength of the pulse. Generally, $H(d)$ is the superposition of the optical channel and target channel responses: $H(d) = H_O(d)\,H_T(d)$. The following equation can be used to represent $H_O(d)$:

$$H_O(d) = \frac{T^2(d)}{d^2}\xi(d) \tag{3}$$

$\xi(d)$ is the optical crossover function between the transmitter and the receiver. It can be represented as a piecewise function in Eq. 4. As we can seen in Fig. 3., D_1 and D_2 are internal parameters serving as function boundaries. D_2 never exceed 2 meters. Therefore, we can safely consider $\xi(d)$ to be 1 for most distance d.

$$\xi(d) = \begin{cases} 0 & , \quad d \le D_1 \\ \frac{d}{D_2 - D_1} - \frac{D_1}{D_2 - D_1}, & D_1 < d < D_2 \\ 1 & , \quad D_2 \le d. \end{cases} \tag{4}$$

$T(d)$ is the one-way atmospheric transmittance of the light beam. Transmittance is associated with the attenuation coefficient α during measurement: $T(d) = \exp(-\alpha d)$. α remains constant in homogeneous optical medium. Koschmieder's law [31] indicates its correlation with fog visibility. On clear days, it can be approximated as 0.

During scanning, the laser beam immediately undergoes reflection upon hitting real targets. Therefore, the target located at distance d_0 has the following impulse response:

$$H_T(d) = H_T^{\text{real}}(d) = \beta_0 \delta(d - d_0) \tag{5}$$

β_0 stands for the reflectivity of the target. It is solely dependent on the properties of the target. Thus, with Eq. 3. and Eq. 5., we can express the total pulse response function originating from the real target as follows:

$$H(d) = \frac{\xi(d_0)}{{d_0}^2}\beta_0 \delta(d - d_0) \tag{6}$$

B. Fog Attenuation Coefficient Estimation

In this section, we estimate α by using a road surface prior knowledge: the detection range of LiDAR never exceeds 200 meters. Within this distance, road is constructed from the same material. The road surface possesses nearly identical reflectivity β_0.

In the presence of fog, the received signal $E_R(d)$ is the combination of two parts: the echo from the real target and the false echo from fog particles.

$$E_R(d) = E_{R,\text{real}}(d) + E_{R,\text{noise}}(d). \tag{7}$$

Due to changes in transmittance, the echo intensity from a real target in foggy weather is attenuated by a factor of $exp(-2\alpha R_0)$ compared to the echo intensity in clear weather [16]. This is because in Time-of-Flight (TOF) LiDAR, the distance the transmitted light travels to the target and the reflected light returns to the receiver is the same. Combining Eq. 6., we can obtain the following equation:

$$E_{R,\text{real}}(d_0) = \frac{C_A E_0 \beta_0}{{d_0}^2} exp(-2\alpha d_0) \tag{8}$$

This equation aligns with the results presented in [9] and [16]. Given the road surface prior fact mentioned above, our method defines the following representation:

$$S(d_0) = \ln \frac{{d_0}^2 E_{R,\text{fog}}^{\text{road}}(d_0)}{C_A E_0} \tag{9}$$

When selecting returned points from two distances (d1 and d2) on road surface like Fig. 4., the echo intensities of these two points, denoted by E_1 and E_2 can be read from the received signal. It should be noted that the values of these intensities do not directly conform to the calculation

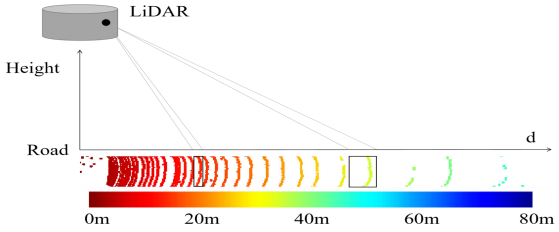

Fig. 4. Selection of Road Surface Points Sets

in Eq. 8.. For normalization purpose, LiDAR manufacturers generally apply specific calibration tables to modify the intensities received [18]. They typically explain this factory-side calibration in user's manual [36]. Therefore, before we proceed with calculations using these intensities, it's necessary to recover the effects of the factory-side calibration like [17]. Then for the chosen road points:

$$S_2 - S_1 = \ln \frac{C_{A1}E_{01}}{C_{A2}E_{02}} - 2\alpha(d_2 - d_1) \tag{10}$$

As explained in Section III.A, $C_{A1}E_{01}$ and $C_{A2}E_{02}$ respectively represent the intrinsic constant of LiDAR scanning layer corresponding to the two chosen points. For a specific type of LiDAR, these parameters remain constant. Upon performing a straightforward simplification and substituting $\ln \frac{C_{A1}E_{01}}{C_{A2}E_{02}}$ with K, α can be expressed as follows:

$$\alpha = \left| \frac{\Delta S - K}{2\Delta d} \right| \tag{11}$$

As far as we know, several algorithms [32]–[34] have achieved efficient and accurate road segmentation in autonomous driving. Our experiments employ the RANSAC [32], primarily due to its efficiency. In real traffic scenarios, the road surface might contain small debris, with slightly varying reflectivity compared to the road surface itself. To minimize the impact of this factor, our method calculate the mean distance d and intensity E for road points along the same scanning layer. The computed results are then used as inputs for Eq. 11.. This step significantly enhances the stability of the algorithm.

C. Distribution of Fog-induced Points

As described above, the attenuation coefficient α is associated with visibility. It signifies the concentration level of fog. In conditions of varying visibility, fog noise exhibits distinct distributions accordingly. Our method investigates the response function of fog droplets in order to establish a connection between the attenuation coefficient and the distribution of fog-induced points.

Typically, the response function of fog droplets follows the Heaviside function, denoted as $H_T^{\text{fog}}(d_0) = \beta U(d_0 - d)$. Here, β represents the backscatter coefficient. It has a specific ratio relationship with the attenuation coefficient α known as the LiDAR ratio [35], denoted as $S_a = \alpha/\beta$. As in the work of pioneers [5], it's value is 65.22. Subsequently, Eq. 1. is employed to calculate the echo of fog to LiDAR. The calculation result is as follows:

$$E_{R,\text{noise}}(d) = C_A E_0 \beta \int_0^{2\tau_H} \sin^2\left(\frac{\pi}{2\tau_H}t\right) \times \frac{\exp\left(-2\alpha\left(d - \frac{ct}{2}\right)\right)}{\left(d - \frac{ct}{2}\right)^2} \xi(d - \frac{ct}{2}) U(d_0 - d + \frac{ct}{2}) dt \tag{12}$$

This is an integral equation solely dependent on visibility V(α, β), distance d, and internal parameters of the sensor. While closed-form computation is not feasible, numerical integration methods can be employed to calculate spurious returns at a certain distance d. The fog noise distribution plot in Fig. 1. showcases the curve of Eq. 12..

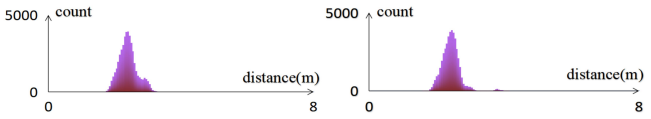

Fig. 5. The noise distribution of the number of fog-induced points with distance calculated from real foggy weather point clouds that we collect. Similar to the distribution in [12].

A Livox-Avia LiDAR is employed to capture point clouds in natural dense fog. Fig. 5. shows the histogram of the number of noise points in discrete 0.05-meter intervals within the efficient response distance. LiDAR employs an undisclosed triggering mechanism, where the probability of triggering is closely tied to the distribution of the echo. As a result, the distribution of noise points with distance roughly follows the same curve as Eq. 12.. The noise distribution shown in [12] and Fig. 5., along with the similarity to the curve of Noise Distribution (ND) in Fig. 1., corroborates this connection.

D. Point Cloud Defogging

Our defogging method constitutes a significant enhancement of Statistical Outlier Removal (SOR) in foggy conditions. A function using Fast Library for Approximate Nearest Neighbors (FLANN) is firstly employed to construct K-D tree. Through K-Nearest Neighbor search for each point, the mean distance M_d to its neighbors, global mean distance μ and standard deviation ν can be acquired. The basic SOR uses a threshold $T_s = \mu + \nu \times constant$. Points with M_d less than T_s are considered noise points. However, the spatially non-uniform distribution of the point cloud leads to its error, as depicted in [19]. This is where DROR [19] and DSOR [20] comes into play. They introduce $T_d = distance \times r \times T_s$ as a new threshold. Inspired by DSOR [19] and DDIOR [21], our approach similarly incorporates distance as the Spatial Distribution (SD). We propose a new threshold T_f for point at certain distance d that effectively merges both distributions:

$$T_f = \sigma \times r \times T_s = (1/ND(d) + d) \times r \times T_s \tag{13}$$

Points with M_d less than T_f are considered to be fog noise and removed. As described in DSOR [20], r is a constant, a multiplicative factor for defogging threshold. A value of r that is too small would make the filter overly aggressive.

IV. EXPERIMENTS

A. Implementation Details

The experiments of this paper comprise two distinct aspects. Firstly, a comparison between our method and SOR [14], DROR [19], DSOR [20] and DDIOR [21] for Precision, Recall and F1-score is conducted on a semi-synthetic foggy dataset. These metrics are common benchmarks for point cloud denoising. Currently, the fog simulation approaches [16] [28] [29], notably [16], have achieved remarkable success in terms of interpretability and realism. Since there is no suitable data labeled for foggy conditions point by point, using this approach to create a dataset for evaluation can provide the required ground truth. Secondly, a 3D object detection experiment is undertaken to assess the impact of different methods on detection task. This experiment employs noisy data captured in real foggy weather scenarios. The results of the 3D object detection serve to emphasize the necessity of defogging for robust autonomous driving in adverse weather conditions.

The experiments are performed on the SeeingThroughFog (STF) dataset [28]. It is a multi-sensor fusion dataset for various weather conditions in autonomous driving. This dataset includes 3,469 training frames captured under clear weather , along with 781 validation frames and 1,847 testing frames specifically for clear weather. The STF dataset also contains 887 testing frames of dense foggy split, capturing real-world foggy weather autonomous driving scenarios. The dataset includes 3D bounding box labels for common objects like cars, pedestrians, and other road traffic elements. This labels facilitates our 3D object detection experiments.

The experiments are conducted on a server with an Intel Xeon(R) Platinum 8375C CPU and two RTX 3090 GPUs. In all experiments, the number of neighbors for K-nearest neighbors searching is set to 5. The standard deviation adjustment constant is set to 0.001 as in [20]. The constant r for threshold T_f is set to 0.062. The value of K in Eq. 11. is set to ln8 to obtain the best results. This internal parameter values can be obtained through calibration for a specific lidar. The half-wave length τ_H, following the Velodyne HDL64 S3D user manual [36], is set to 10ns [17]. The system constant in Eq. 12. is set to 5e11 to get relatively accurate distribution. The presence of r makes the setting of this parameter value less critical.

B. Defogging

The defogging experiment uses the testing split of STF dataset. The fog simulation method proposed in [16] is applied to add fog noise on all 1847 frames in the test split. This simulated ground truth facilitates the computation of True Positives (TP), True Negatives (TN), False Negatives (FN), and False Positives (FP) for evaluation. Commonly used metrics in point cloud denoising, namely precision, recall, and F1-score, are employed for performance assessment. The calculation methods for these metrics are as follows:

$$Precision = \frac{TP}{TP + FP}$$

$$Recall = \frac{TP}{TP + FN}$$

$$F1 - Score = \frac{2Precision * Recall}{Precision + Recall}$$

The SOR [14], DROR [19], DSOR [20] and DDIOR [21] methods are employed for comparison. DDIOR [21] is mainly used to demonstrate that intensity-based defogging methods may fail in foggy weather. Table 1 lists the results of each algorithm.

TABLE I. COMPARISON BETWEEN DEFOGGING METHODS

	Precision	Recall	F1-Score
SOR [14]	12.74%	72.38%	21.67%
DROR [19]	62.54%	92.95%	74.77%
DSOR [20]	61.95%	90.70%	73.62%
DDIOR [21]	13.96%	**94.34%**	24.32%
Ours	**70.92%**	90.01%	**79.33%**

Table I shows that all methods achieve a relatively high recall rate. This indicates their ability to identify fog-noise points. However, the traditional SOR method used in [14] exhibits the lowest precision. This suggests that it erroneously removes a significant number of points originating from real targets. The precision of DDIOR is also quite low. This is because the intensity of real target points is close to that of fog-induced points, as explained in Section II.C. Our method demonstrates the highest precision, surpassing others. Correspondingly, on the composite metric F1-Score our method also achieves the highest value. This exceptional performance can be attributed to the fact that our method takes the distribution of fog noise into account. The reasonable design allows our method to make more precise and accurate distinctions between noise and real target points.

Nevertheless, due to its intrinsic chain of road segmentation, fog coefficient estimation and denoising dependent on noise distribution, the method introduces considerable latency before generating usable clear point clouds. The time overhead measured in our experiments is approximately 9.3 times that of DSOR method (182.9ms vs. DSOR's 19.6ms for a frame with about 14000 points). However, future improvements could significantly accelerate the process by reducing the frequency of attenuation coefficient estimation and repetitive noise distribution computations.

C. 3D Object Detection

3D object detection experiments are conducted using the Voxel-RCNN [2] detection network. It exhibits outstanding performance across various 3D object detection datasets. The network is trained using all the clear weather train split from the STF dataset. All of the dense fog frames are used for testing. Evaluation is based on standard KITTI metrics [37], encompassing 3D and Bird's Eye View (BEV) metrics. Table II compares the results of the baseline without defogging and the results of defogging by different methods. Our approach is compared against other unsupervised adverse weather denoising algorithms.

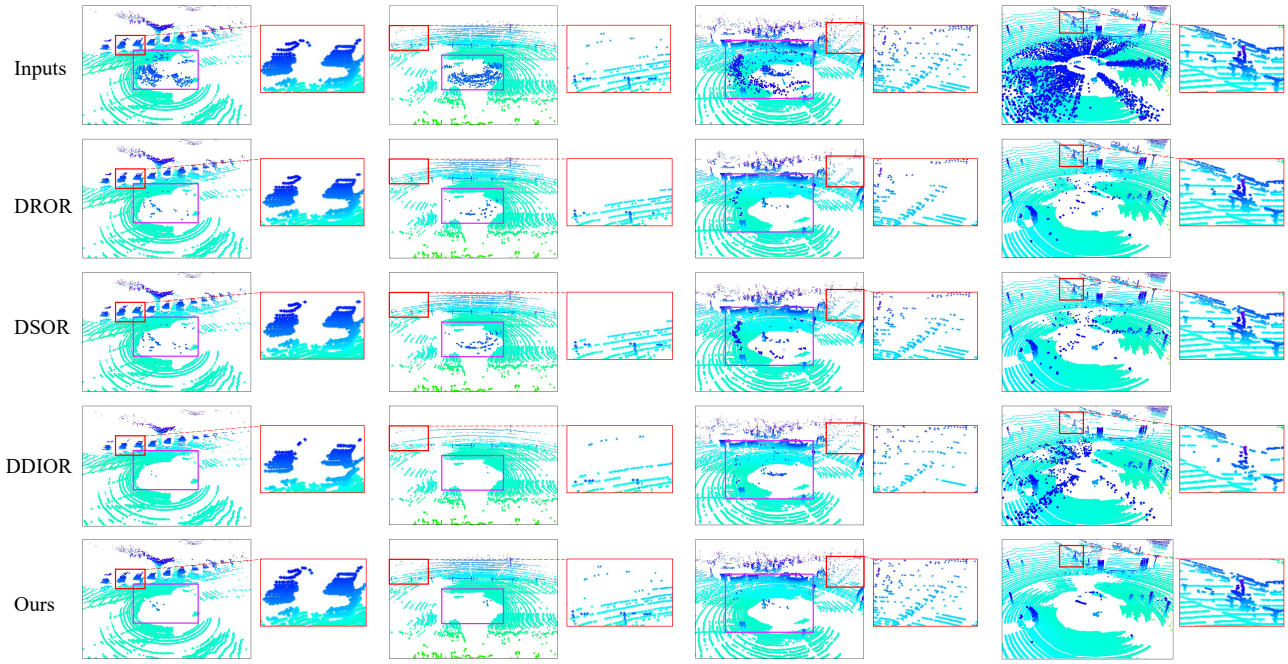

Fig. 6. Defogging effects with different methods. Noise points Purple boxes represent recall and real target points in red boxes represent precision. The first three columns use data captured in authentic foggy weather scenarios from STF dataset [28], while the last column uses fog weather data generated by [16]. The results for DROR [19] and DSOR [20] indicate that when important real target points start disappearing, a significant amount of noise still remains. DDIOR [21] mistakenly filter out points from real targets to a severe extent due to the difference in noise intensity between fog and snow.

TABLE II. 3D OBJECT DETECTION RESULTS

	Methods	Car .5IOU				Pedestrian .25IOU				
		Easy	Moderate	Hard	mAP	Easy	Moderate	Hard	mAP	Average
BEV Metric	baseline	33.77%	36.22%	37.53%	35.84%	29.00%	29.09%	29.76%	29.28%	32.56%
	SOR [14]	27.91%	29.37%	29.86%	29.05%	17.14%	16.55%	17.09%	16.93%	22.99%
	DROR [19]	35.26%	36.78%	37.56%	36.53%	29.17%	**29.61%**	30.01%	**29.60%**	33.07%
	DSOR [20]	35.56%	37.53%	38.04%	37.04%	**29.27%**	29.33%	**30.17%**	29.59%	33.32%
	DDIOR [21]	32.56%	34.79%	35.75%	34.37%	26.81%	27.07%	27.40%	27.09%	30.73%
	Ours	**36.17%**	**38.30%**	**38.82%**	**37.76%**	28.86%	29.21%	29.83%	29.30%	**33.53%**
3D Metric	baseline	27.88%	29.96%	31.42%	29.75%	28.71%	26.20%	26.85%	27.25%	28.50%
	SOR [14]	22.99%	24.31%	24.71%	24.00%	16.81%	16.11%	16.88%	16.60%	20.30%
	DROR [19]	29.72%	31.65%	32.40%	31.26%	28.14%	28.29%	28.87%	28.43%	29.85%
	DSOR [20]	29.96%	31.82%	32.65%	31.48%	**28.17%**	**28.46%**	**28.89%**	**28.51%**	29.99%
	DDIOR [21]	24.72%	26.97%	28.00%	26.56%	26.32%	25.93%	26.27%	26.17%	26.39%
	Ours	**30.51%**	**34.29%**	**35.34%**	**33.38%**	27.93%	28.09%	28.82%	28.28%	**30.83%**

The results show that our method achieves the best on both metrics on average. This aligns with the results in Table I and Fig. 6.. This indicates that our method is equally accurate on real foggy weather data. It's important to note that fog-induced noise is limited, and the network has inherent noise discrimination. Removing all of this noise doesn't drastically improve the performance of 3D object detection. Despite this, our method improves the detection of car compared to the baseline and other methods. For pedestrian detection, differences between methods are minor, likely due to few pedestrians in fog-affected areas. On average, our method enhances the performance of the detection network.

V. CONCLUSIONS

In this work, we propose a machine learning defogging method for autonomous driving under foggy weather conditions. The motivation is that the distribution of noise varies with changes in visibility. Our method estimates the fog attenuation coefficient α from a single-frame point cloud. α is then utilized in LiDAR imaging model to acquire the distribution of fog-induced noise. Drawing inspiration from several successful noise sparsity-based methods, the distribution of noise and the system's non-uniform distribution work in conjunction to achieve accurate defogging. Experimental results demonstrate that our method possesses noteworthy fog removal capability and enhances the performance of 3D object detection network operating in foggy weather. Though our method may impose additional computational complexity, we can address this issue in the future by establishing a mapping table or training an MLP network. The main insight of this paper lies in proposing the defogging framework based on the estimation of the visibility-related attenuation coefficient and noise distribution in foggy weather. We expect that our proposed method can find extensive applications across diverse domains dealing with fog-induced challenges in the foreseeable future.

REFERENCES

[1] Y. Yan, Y. Mao, and B. Li, "Second: Sparsely embedded convolutional detection," *Sensors*, vol. 18, no. 10, p. 3337, 2018.

[2] J. Deng, S. Shi, P. Li, W. Zhou, Y. Zhang, and H. Li, "Voxel r-cnn: Towards high performance voxel-based 3d object detection," in *Proceedings of the AAAI Conference on Artificial Intelligence*, vol. 35, no. 2, 2021, pp. 1201–1209.

[3] M.-F. Chang, J. Lambert, P. Sangkloy, J. Singh, S. Bak, A. Hartnett, D. Wang, P. Carr, S. Lucey, D. Ramanan *et al.*, "Argoverse: 3d tracking and forecasting with rich maps," in *Proceedings of the IEEE/CVF conference on computer vision and pattern recognition*, 2019, pp. 8748–8757.

[4] J. Cheng, L. Zhang, Q. Chen, X. Hu, and J. Cai, "A review of visual slam methods for autonomous driving vehicles," *Engineering Applications of Artificial Intelligence*, vol. 114, p. 104992, 2022.

[5] R. H. Rasshofer, M. Spies, and H. Spies, "Influences of weather phenomena on automotive laser radar systems," *Advances in radio science*, vol. 9, pp. 49–60, 2011.

[6] M. Bijelic, T. Gruber, and W. Ritter, "A benchmark for lidar sensors in fog: Is detection breaking down?" in *2018 IEEE Intelligent Vehicles Symposium (IV)*. IEEE, 2018, pp. 760–767.

[7] M. Kutila, P. Pyykönen, H. Holzhüter, M. Colomb, and P. Duthon, "Automotive lidar performance verification in fog and rain," in *2018 21st International Conference on Intelligent Transportation Systems (ITSC)*. IEEE, 2018, pp. 1695–1701.

[8] Y. Li, P. Duthon, M. Colomb, and J. Ibanez-Guzman, "What happens for a tof lidar in fog?" *IEEE Transactions on Intelligent Transportation Systems*, vol. 22, no. 11, pp. 6670–6681, 2020.

[9] T. Yang, Y. Li, Y. Ruichek, and Z. Yan, "Lanoising: A data-driven approach for 903nm tof lidar performance modeling under fog," in *2020 IEEE/RSJ International Conference on Intelligent Robots and Systems (IROS)*. IEEE, 2020, pp. 10 084–10 091.

[10] T. Yang, Y. Li, Y. Ruichek, and Z. Yan, "Performance modeling a near-infrared tof lidar under fog: A data-driven approach," *IEEE Transactions on Intelligent Transportation Systems*, vol. 23, no. 8, pp. 11 227–11 236, 2021.

[11] K. Montalban, C. Reymann, D. Atchuthan, P.-E. Dupouy, N. Riviere, and S. Lacroix, "A quantitative analysis of point clouds from automotive lidars exposed to artificial rain and fog," *Atmosphere*, vol. 12, no. 6, p. 738, 2021.

[12] K. Montalban, C. Reymann, D. Atchuthan, P.-E. Dupouy, N. Rivière, and S. Lacroix, "Bayesian inference of fog visibility from lidar point clouds and correlation with probabilities of detection," in *2023 IEEE International Conference on Robotics and Automation (ICRA)*. IEEE, 2023, pp. 7076–7082.

[13] A. U. Shamsudin, K. Ohno, T. Westfechtel, S. Takahiro, Y. Okada, and S. Tadokoro, "Fog removal using laser beam penetration, laser intensity, and geometrical features for 3d measurements in fog-filled room," *Advanced robotics*, vol. 30, no. 11-12, pp. 729–743, 2016.

[14] S.-L. Lin and B.-H. Wu, "Application of kalman filter to improve 3d lidar signals of autonomous vehicles in adverse weather," *Applied Sciences*, vol. 11, no. 7, p. 3018, 2021.

[15] R. Heinzler, F. Piewak, P. Schindler, and W. Stork, "Cnn-based lidar point cloud de-noising in adverse weather," *IEEE Robotics and Automation Letters*, vol. 5, no. 2, pp. 2514–2521, 2020.

[16] M. Hahner, C. Sakaridis, D. Dai, and L. Van Gool, "Fog simulation on real lidar point clouds for 3d object detection in adverse weather," in *Proceedings of the IEEE/CVF International Conference on Computer Vision*, 2021, pp. 15 283–15 292.

[17] M. Hahner, C. Sakaridis, M. Bijelic, F. Heide, F. Yu, D. Dai, and L. Van Gool, "Lidar snowfall simulation for robust 3d object detection," in *Proceedings of the IEEE/CVF Conference on Computer Vision and Pattern Recognition*, 2022, pp. 16 364–16 374.

[18] Q. Ding, W. Chen, B. King, Y. Liu, and G. Liu, "Combination of overlap-driven adjustment and phong model for lidar intensity correction," *ISPRS journal of photogrammetry and remote sensing*, vol. 75, pp. 40–47, 2013.

[19] N. Charron, S. Phillips, and S. L. Waslander, "De-noising of lidar point clouds corrupted by snowfall," in *2018 15th Conference on Computer and Robot Vision (CRV)*. IEEE, 2018, pp. 254–261.

[20] A. Kurup and J. Bos, "Dsor: A scalable statistical filter for removing falling snow from lidar point clouds in severe winter weather," *arXiv preprint arXiv:2109.07078*, 2021.

[21] W. Wang, X. You, L. Chen, J. Tian, F. Tang, and L. Zhang, "A scalable and accurate de-snowing algorithm for lidar point clouds in winter," *Remote Sensing*, vol. 14, no. 6, p. 1468, 2022.

[22] J.-I. Park, J. Park, and K.-S. Kim, "Fast and accurate desnowing algorithm for lidar point clouds," *IEEE Access*, vol. 8, pp. 160 202–160 212, 2020.

[23] M.-Y. Yu, R. Vasudevan, and M. Johnson-Roberson, "Lisnownet: Real-time snow removal for lidar point clouds," in *2022 IEEE/RSJ International Conference on Intelligent Robots and Systems (IROS)*. IEEE, 2022, pp. 6820–6826.

[24] B. Li, J. Li, G. Chen, H. Wu, and K. Huang, "De-snowing lidar point clouds with intensity and spatial-temporal features," in *2022 International Conference on Robotics and Automation (ICRA)*. IEEE, 2022, pp. 2359–2365.

[25] A. Seppänen, R. Ojala, and K. Tammi, "4denoisenet: Adverse weather denoising from adjacent point clouds," *IEEE Robotics and Automation Letters*, vol. 8, no. 1, pp. 456–463, 2022.

[26] A. Seppänen, R. Ojala, and K. Tammi, "Multi-echo denoising in adverse weather," *arXiv preprint arXiv:2305.14008*, 2023.

[27] A. Carballo, J. Lambert, A. Monrroy, D. Wong, P. Narksri, Y. Kitsukawa, E. Takeuchi, S. Kato, and K. Takeda, "Libre: The multiple 3d lidar dataset," in *2020 IEEE Intelligent Vehicles Symposium (IV)*. IEEE, 2020, pp. 1094–1101.

[28] M. Bijelic, T. Gruber, F. Mannan, F. Kraus, W. Ritter, K. Dietmayer, and F. Heide, "Seeing through fog without seeing fog: Deep multimodal sensor fusion in unseen adverse weather," in *Proceedings of the IEEE/CVF Conference on Computer Vision and Pattern Recognition*, 2020, pp. 11 682–11 692.

[29] V. Kilic, D. Hegde, V. Sindagi, A. B. Cooper, M. A. Foster, and V. M. Patel, "Lidar light scattering augmentation (lisa): Physics-based simulation of adverse weather conditions for 3d object detection," *arXiv preprint arXiv:2107.07004*, 2021.

[30] P. Duthon, M. Colomb, and F. Bernardin, "Light transmission in fog: The influence of wavelength on the extinction coefficient," *Applied Sciences*, vol. 9, no. 14, p. 2843, 2019.

[31] N. Hautiere, J.-P. Tarel, J. Lavenant, and D. Aubert, "Automatic fog detection and estimation of visibility distance through use of an onboard camera," *Machine vision and applications*, vol. 17, no. 1, pp. 8–20, 2006.

[32] M. A. Fischler and R. C. Bolles, "Random sample consensus: a paradigm for model fitting with applications to image analysis and automated cartography," *Communications of the ACM*, vol. 24, no. 6, pp. 381–395, 1981.

[33] Y. Zhang, J. Wang, X. Wang, and J. M. Dolan, "Road-segmentation-based curb detection method for self-driving via a 3d-lidar sensor," *IEEE transactions on intelligent transportation systems*, vol. 19, no. 12, pp. 3981–3991, 2018.

[34] E. E. Aksoy, S. Baci, and S. Cavdar, "Salsanet: Fast road and vehicle segmentation in lidar point clouds for autonomous driving," in *2020 IEEE intelligent vehicles symposium (IV)*. IEEE, 2020, pp. 926–932.

[35] W. Gong, J. Zhang, F. Mao, and J. Li, "Measurements for profiles of aerosol extinction coeffcient, backscatter coeffcient, and lidar ratio over wuhan in china with raman/mie lidar," *Chinese Optics Letters*, vol. 8, no. 6, pp. 533–536, 2010.

[36] Velodyne. ,"Hdl-64e user's manual," 2007,

[37] A. Geiger, P. Lenz, and R. Urtasun, "Are we ready for autonomous driving? the kitti vision benchmark suite," in *2012 IEEE Conference on Computer Vision and Pattern Recognition*, 2012, pp. 3354–3361.